JTTEE5 20:83–91
DOI: 10.1007/s11666-010-9589-6
1059-9630/$19.00 © ASM International

Phase Composition and Microstructural Responses of Graded Mullite/YSZ Coatings Under Water Vapor Environments

E. Garcia, J. Mesquita-Guimarães, P. Miranzo, M.I. Osendi, C.V. Cojocaru, Y. Wang, C. Moreau, and R.S. Lima

(Submitted April 29, 2010; in revised form October 5, 2010)

Mullite-based systems have been considered as environmental barrier coatings (EBCs) for high temperature protection of Si-based ceramic (Si_3N_4, SiC) substrates against water vapor corrosion, for application in forthcoming turbine engines. Graded mullite/Y-ZrO_2 composites plasma sprayed over Hexoloy SiC substrates were analyzed as EBCs. All feedstock materials were purposely prepared and singular spraying conditions were used to assure superior crystallization. The different coated specimens were subjected to temperatures of 1300 °C for 100-500 h under water vapor environment. The effect of water corrosion on the exposed coatings was investigated by focusing on their phase and microstructure changes.

Keywords environmental barrier coating, graded mullite/ZrO_2, layered coatings, plasma spray, thermal aging, water vapor corrosion

1. Introduction

Various single layer and multilayered environmental barrier coatings (EBCs) have been intended to protect Si-based ceramic (Si_3N_4, SiC) components of gas turbines against severe conditions, in particular, water vapor and high temperatures (Ref 1, 2). For this purpose, mullite coatings have been tried either as a single or intermediate layer in the EBC systems (Ref 1-5) because of its low density, low thermal conductivity, stability in oxidizing environments and its thermal expansion coefficient that is close to those of Si_3N_4 and SiC. Plasma sprayed mullite coatings commonly develop high amount of amorphous phase, which after thermal exposure crystallizes producing extensive cracking (Ref 3, 4). Efforts have been put into reducing the presence of amorphous phases in the coatings by raising the substrate temperature during thermal spraying (Ref 4, 5), thus generally enhancing their mechanical integrity. Nevertheless, even fully crystalline mullite coatings exhibited some silica volatilization and alumina scale formation under high pressure steam atmospheres (Ref 5). Consequently, different solutions based on mullite have been tried to improve the coating lifetime in this harsh environment. A 7 wt.% Y_2O_3-ZrO_2 (YSZ) top coat (Ref 5) plasma sprayed on the first mullite layer showed good adhesion and air oxidation resistance, but the large thermal expansion mismatch between YSZ and mullite layers caused extensive cracking and the formation of a porous silica scale after 200 h of exposure at temperatures of 1300 °C in a water vapor-rich atmosphere. Multilayered systems based on mullite + barium and strontium aluminum silicate (BSAS) and mullite + rare earth aluminum silicates (Ref 6, 7) have recently been designed with good crack resistance, although they showed volatilization at temperatures of 1300 °C under harsh combustion conditions (Ref 8, 9).

On the other hand, a 7 wt.% Y_2O_3-ZrO_2/mullite composite coating tested as a thermal barrier coating (TBC) on a metal substrate showed a considerable increase in creep resistance (Ref 10). Therefore, with the rationale of maintaining the system as simple as possible regarding the number of components, and bearing in mind that ZrO_2 has a low volatility in water vapor environments (Ref 5) and mullite is compatible and shows good adherence to SiC, we have chosen mullite/YSZ composite coatings as a protective system. Aiming to reduce through-thickness cracks due to thermal expansion mismatch between mullite and YSZ layers, intermediate composite layers with graded compositions have been designed and plasma sprayed on a pure mullite bonding layer. The reduction in the formation of amorphous mullite was also a key issue as the crystallization of mullite during the high temperature treatments produced extensive microcraking (Ref 3).

This article is an invited paper selected from presentations at the 2010 International Thermal Spray Conference and has been expanded from the original presentation. It is simultaneously published in *Thermal Spray: Global Solutions for Future Applications, Proceedings of the 2010 International Thermal Spray Conference*, Singapore, May 3-5, 2010, Basil R. Marple, Arvind Agarwal, Margaret M. Hyland, Yuk-Chiu Lau, Chang-Jiu Li, Rogerio S. Lima, and Ghislain Montavon, Ed., ASM International, Materials Park, OH, 2011.

E. Garcia, J. Mesquita-Guimarães, P. Miranzo, and **M.I. Osendi**, Institute of Ceramics and Glass (ICV), CSIC, Madrid, Spain; and **C.V. Cojocaru**, **Y. Wang**, **C. Moreau**, and **R.S. Lima**, National Research Council of Canada (NRC), Boucherville, QC, Canada. Contact e-mail: miosendi@icv.csic.es.

Because these mix compositions were not commercially available, mullite/Y-ZrO_2 powders were first prepared and subsequently plasma sprayed over Hexoloy SiC substrates following a specific procedure to achieve quite crystalline graded mullite/Y-ZrO_2 coatings. Single mullite coatings were used as a control specimen. Coated specimens were subjected to water vapor-rich atmospheres at 1300 °C, up to 500 h. The purpose of this study is to analyze the effect of exposure on the microstructure and phases of the specimens, compared to the as-sprayed coatings. The differences were explored using different analytical techniques, electron microscopy observations, and differential thermal analysis.

2. Experimental

Mullite ($3Al_2O_3{\cdot}2SiO_2$) powders (Baikalox SASM, Baikowski Chemie, Annecy, France) with a purity of 99% of mullite phase and an average particle size of 1.3 μm and tetragonal zirconia powders stabilized with 7 wt.% Y_2O_3 (TZ4Y, Tosoh, Tokyo, Japan), with a reported purity of 99.95% and an average particle size of 0.3 μm, were used as starting materials. Suspensions with 30 wt.% of solid contents of mullite and mullite/Y-ZrO_2 mixtures were prepared and spray dried (SD), in the same way as described in a previous work (Ref 11), to get the feedstock powders with a particle size of −60/+5 μm. Alternatively, a batch of mullite was prepared following a CSIC proprietary freeze-granulation (FG) method from the same starting powders; the particle size of the FG feedstock was −150/+32 μm. Compositions were labeled as M100 (plain mullite), M75 (75 vol.% mullite-25 vol.% Y-ZrO_2) and M50 (50 vol.% mullite-50 vol.% Y-ZrO_2).

Feedstock powders were air plasma sprayed (APS) with an Axial III plasma torch (Northwest Mettech, North Vancouver, BC, Canada) on 5 × 5 cm SiC substrates (Hexoloy SA, Saint-Gobain, Worcester, MA, USA) under proprietary spray conditions. The substrate temperature was continuously checked to assure a maximum crystallization of the mullite phase using a proprietary NRC technology. Single coatings of M100 from the SD batch were directly sprayed over the SiC. An additional layer was plasma sprayed on part of these coatings for achieving bi-layer (M100/M75) systems. In the three-layer (M100/M75/M50) coatings, the mullite bond coat was sprayed from the FG batch and the other two layers were sequentially sprayed from SD powders over the mullite layer. The temperature and velocity of the particles were monitored in-flight with a DPV-2000 diagnostic system (Tecnar Automation, St-Bruno, QC, Canada). For subsequent aging tests, specimens were cut in four samples of 2.5 × 2.5 cm using metal-bonded diamond blades. Aging consisted of isothermal exposure at 1300 °C for 100 and 500 h, in a water vapor environment (90% H_2O/10% air) at 1 atm of pressure under a continuous flow of 3.5 cm/s, using the NRC Boucherville in-house developed rig based on a high-temperature tube furnace (STT-1700-2.0-18, SentroTech, Cleveland, OH, USA). For the control single mullite coatings, only aging tests of 100 h were completed as its behavior is well known (Ref 3-5).

For the microstructure analysis of as-sprayed and aged coatings, cross-sections of the specimens were cut, ground, and polished using diamond polishing compounds. The microstructures of the coatings were viewed with a field emission scanning electron microscope (FEM, Hitachi 4700, Tokyo, Japan). Point and area microanalyses were done using x-ray energy dispersive spectroscopy (EDS, Thermo Noran, System SIX, Madison, WI, USA) and quantitative results were obtained using the ZAF (atomic number, absorption, fluorescence) correction software and theoretical internal standards. For the area analysis, probe zones of 70 × 70 μm and 40 × 40 μm were used depending on the layer thickness. Analysis of specific layers (M100, M75, M50) were also done by electron probe microanalysis (EPMA, Jeol JXA 8900) across the coatings using standards. To be confident that the area microanalyses correctly reproduced the average coating compositions, x-ray fluorescence (XRF, MagiX Pro; Phillips, Eindhoven, Netherlands) analyses were done on the original powders, and the data was compared with EDS area microanalysis carried out for dense specimens sintered from the same powders. Results from the different methods (EPMA, XRF, area EDS) were coincident within the experimental scattering and, therefore, it was assumed that area analysis accurately reflected the average composition within each layer. X-ray diffraction analyses (XRD) were performed on the coating surface using a Xpert PRO diffractometer (PANalytical, Almelo, Netherlands) with a θ/2θ configuration, in the 10-70° 2θ range, with a step of 0.0165, a time per step of 50 s and a rotation speed of 15 rpm. The differential thermal analyses (DTA) were performed on single coatings of each composition, with a Simultaneous Thermal Analyzer (Netzch 409, Bavaria, Germany), at a heating rate of 10 °C/min, using an alumina standard. The specimens for DTA experiments were scraped off the substrates (M100 and M75) or were easily detached in the case of M50 single coating. Porosity in each layer of the graded coatings was estimated using image analysis software over SEM binarized micrographs, counting more than 6000 features per coating.

3. Results and Discussion

In Fig. 1, cross-sectional SEM micrographs of the as-sprayed coatings are shown, where the thicknesses of the M100 single layer, M100/M75 bi-layer and M100/M75/M50 three-layer coatings are 150, 200, and 250 μm, respectively. Low porosity, typically 6, 4, and 9% for the single-, bi-, and three-layer coatings, respectively, was estimated. The relatively higher porosity of the three-layer coatings was due to the weight of the highly porous mullite FG bonding layer (~30%) in this system. This porous mullite layer was intentionally sprayed to provide higher strain tolerance in the three-layer coating. Good adhesion of the mullite layer to the substrate and between the different layers was evidenced; although, the presence of

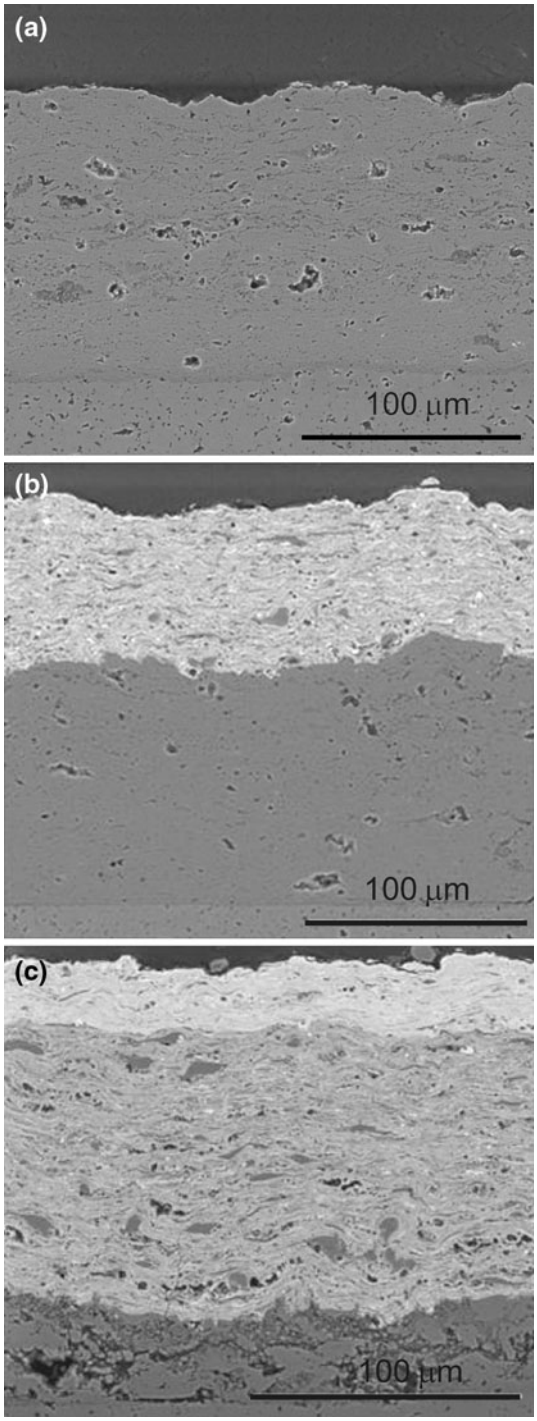

Fig. 1 SEM micrographs of M100 (a), M100/ M75 (b), and M100/ M75/M50 (c) as-sprayed coatings. Mullite bottom layer in coating (c) corresponds to FG batch (see text)

evenly spaced vertical cracks was common for all the coatings that occasionally reached the mullite-SiC interface, especially for the single mullite coating. The formation of cracks can be associated with the thermal expansion mismatch between the coatings and the substrate, and to the high density of these coatings as well.

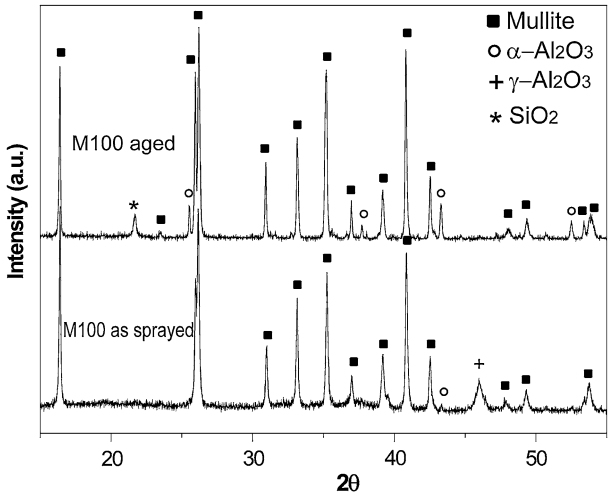

Fig. 2 XRD patterns of M100 coatings: as sprayed (bottom) and 100 h aged (top)

Although these vertical cracks can be a preferential path for the hot gases to reach the substrate (Ref 5), they may partially close at working temperatures. On the other hand, they can provide certain strain tolerance under cycling operation (Ref 12). Figure 2 shows the XRD patterns of the M100 coating, as-sprayed and after 100 h of aging, all plotted at the same scale. The main phase in the as-sprayed coating is mullite but peaks of γ-Al_2O_3 and traces of α-Al_2O_3 are also detected. In the aged M100 sample, mullite is also the major phase but γ-Al_2O_3 is not detected because it probably transformed into α-Al_2O_3 as the relative increase in the peak's intensity seems to indicate. In this sample, a small peak corresponding to cristobalite is noticed, as well.

In Fig. 3, XRD patterns for the M100/M75 bi-layer coatings that just give information of the uppermost layer are plotted. The full-scale intensity of the XRD pattern for the as-sprayed coating is enlarged ($\times 2$) to show similar definition to the other two patterns of the aged samples. Tetragonal ZrO_2 is the main crystalline phase in the as-sprayed coating, whereas characteristics peaks for mullite and γ-Al_2O_3 are hardly detected. Even the stronger ZrO_2 peaks show significant widening, which is an indication, together with the overall low intensity of this pattern, of the feeble crystallinity and the small crystallite size of the M75 top layer. The pattern for the bi-layer coating after 100 h of aging (Fig. 3) shows very intense and sharp peaks of t-ZrO_2 that indicates an increase of the ZrO_2 crystallite size. Furthermore, mullite phase is perfectly detected and small peaks corresponding to α-Al_2O_3 are found as well. For the 500 h treatment, a similar pattern is obtained except for the occurrence of small but clearly detected peaks of zircon ($ZrSiO_4$).

The XRD patterns for the three-layer coatings (M50 top layer) are plotted in Fig. 4 at the same intensity scale. Only t-ZrO_2 peaks are detected for the as-sprayed specimen, which also show some widening. For the aged specimens, patterns with sharp peaks of t-ZrO_2 and lower intensity peaks of mullite, α-Al_2O_3 and $ZrSiO_4$ are detected.

Therefore, these patterns show a similar evolution to those of the bi-layer system (Fig. 3).

The DTA (Fig. 5) of the as-sprayed M100 composition does not show any endothermic or exothermic event that could be associated to crystallization phenomena, supporting the fact that as-sprayed coating is fully crystallized. Conversely, the thermograph for the as-sprayed M75 composition (Fig. 5) revealed the occurrence of two exothermic peaks, at 998 and 1268 °C, whereas a single exothermic peak at 1263 °C was observed for the M50 composition. As mullite crystallization from amorphous mixtures typically gives a strong exothermic peak at ~980 °C (Ref 13, 14) and a lower intensity peak around 1250 °C, DTA results indicate that mullite is comparatively less crystalline for the M75 and M50 than for the pure mullite, given the same spraying conditions, which is in agreement with the XRD results. Therefore, it can be stated that mullite crystallization is hindered in the composites during the spraying process, as has been observed in a previous study on the crystallization of amorphous mullite/ZrO_2 beads (Ref 13). Finally, for aged coatings no crystallization events are recorded in the DTA, being an indication of their higher crystallinity.

The average compositions of the different layers in both the as-sprayed and the aged coatings (Table 1-3) indicated that water vapor exposure does not appreciably change the

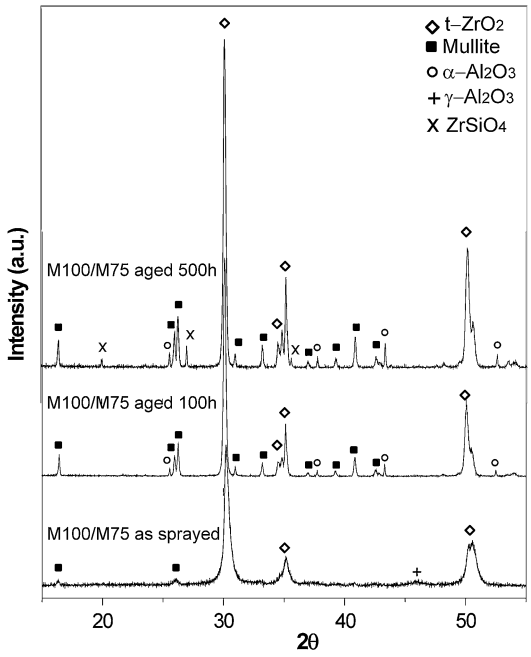

Fig. 3 XRD patterns of as sprayed (bottom), 100 h aged (middle), and 500 h aged (top) bi-layer coating

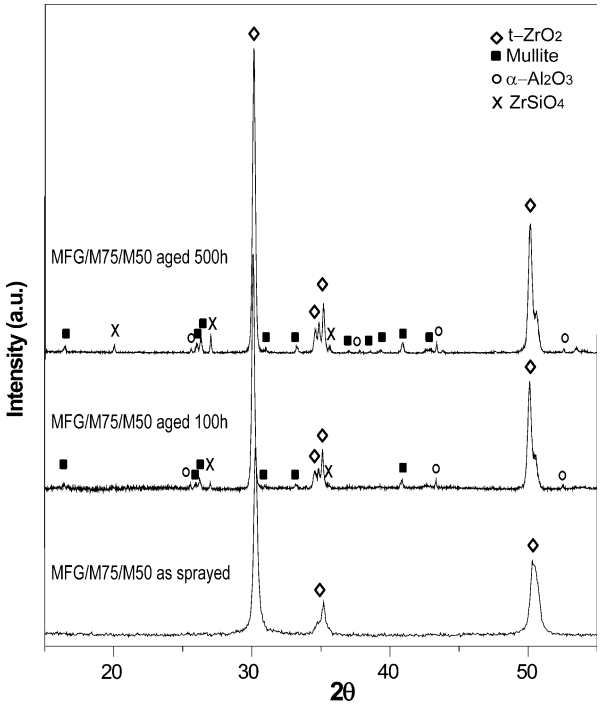

Fig. 4 XRD patterns of the as sprayed (bottom), 100 h aged (middle), and 500 h aged (top) three-layer system

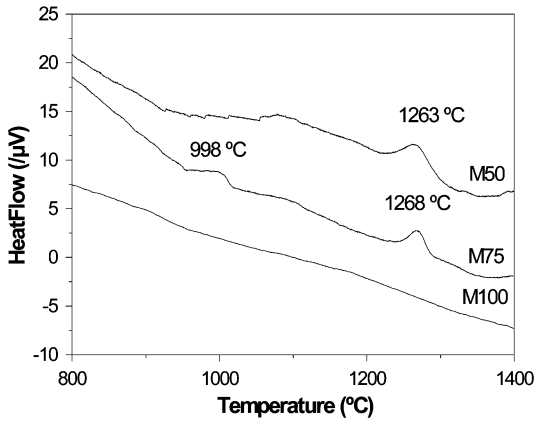

Fig. 5 DTA of as-sprayed coatings for M100, M75, and M50 specimens

Table 1 Area microanalyses of powders and coatings for M100 composition

wt.%	Original	M100AS	M100/100 h	M100/500 h
Al_2O_3	71-72	71-74	72-74	72-74
SiO_2	27-28	26-29	26-28	26-28

Table 2 Area microanalyses of powders and coatings for M75 composition

wt.%	Original	M75AS	M75/100 h	M75/500 h
Al_2O_3	42-45	43-45	41-43	42-50
SiO_2	16-18	11-12	12-14	10-13
Y_2O_3	2.6-3	2.5-3.5	3-4	2-3
ZrO_2	36-39	40-41	40-42	38-43

Table 3 Area microanalyses of powders and coatings for M50 composition

wt.%	Original	M50AS	M50/100 h	M50/500 h
Al_2O_3	23-27	21-23	23-25	22-29
SiO_2	8-10	6-7	7-8	4-8
Y_2O_3	4.5-5.5	5-6	4.5-5	4.5-5
ZrO_2	60-64	65-67	62-65	62-66

chemical composition of each layer. In particular, the data for M100 coatings, summarized in Table 1, show the same chemical composition before and after exposure, which is also identical to the original powder composition. Regarding the composite layers, M75 and M50, the average microanalyses are also practically similar before and after water vapor exposure (see Table 2, 3). Nevertheless, if we compare them to the composition of original powders, a detectable loss of SiO_2 is evident in both coatings, amounting to 5-7 wt.% for M75 composite layer and 2-4 wt.% for the M50 composite layer. Consequently, under the present spraying conditions, the composite coatings showed a silica defective mullite composition. This effect is not due to the possible presence of un-reacted SiO_2 in the original powders as it was not detected in the M100 coatings. Instead, it may be attributed to the lower liquidus temperature of the mixtures, which according to the Al_2O_3-SiO_2-ZrO_2 system would start to melt at temperatures of 1750 °C (Ref 15), i.e., about 100 °C below the mullite melting point. Besides, the presence of ZrO_2 in the compositions hinders the crystallization of mullite (Fig. 5). Consequently, both effects would favor the presence of amorphous phases in the as-sprayed composites thus facilitating silica volatilization in the plasma torch. In fact, an analogous SiO_2 loss effect has been observed for a flame sprayed mullite-ZrO_2 mixture (Ref 14). The higher SiO_2 deficit in the as-sprayed M75 than in the M50 can be just due to the larger mullite content in the original batch composition.

To find out if the formation of $ZrSiO_4$ (Fig. 3) was just a surface effect or takes place across the whole layer, grazing incidence XRD patterns were consecutively recorded for the 500 h aged three-layer coating after stepwise removal of the layers by gently grinding. These XRD patterns are jointly depicted in Fig. 6 at the same scale for the area of interest (25°-30°, 2θ), showing that the formation of $ZrSiO_4$ occurred across the M50 layer and even happened in the M75 layer.

The solid state reaction for the formation of zircon usually occurs above 1400 °C (Ref 16) nevertheless, when Si atoms are transported in a gaseous state, this reaction can take place at temperatures as low as 1000 °C (Ref 17). Besides, in plasma-spheroidized zircon/Al_2O_3 mixtures, the formation of zircon was reported after 10 h of holding at temperatures of 1300 °C (Ref 18), although in that case it was associated to the zircon recombination as this phase was originally present.

In present case, the formation of zircon could be favored by the presence of water vapor as Si can be

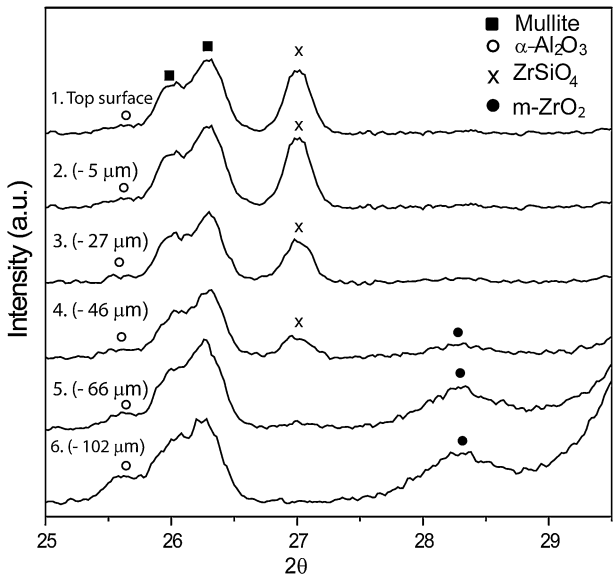

Fig. 6 Grazing incidence XRD patterns of three-layer (M100/M75/M50) coating after sequentially taking off the uppermost layer, removed thickness is given in the parenthesis

transported in a gas state to the ZrO_2 sites, according to following reactions:

$$\left.\begin{array}{l} SiO_2(s) + 2H_2O\,(g) = Si(OH)_4\,(g) \\ Si(OH)_4\,(g) + ZrO_2(s) = ZrSiO_4(s) + 2H_2O\,(g) \end{array}\right\} \quad \text{(Eq 1)}$$

The reactions will give a null mass balance, which would explain the lack of a porous scale in aged specimens.

The microstructures of the as-sprayed and 100 h aged single-layer mullite coatings (M100) are shown in Fig. 7; all display different contrast zones as is usually seen in thermally sprayed mullite (Ref 5). Point microanalyses in the different zones give dissimilar Al_2O_3/SiO_2 ratios (see table inserted in Fig. 7), where the clear elongated white areas (Point 1 in Fig. 7a) typically show higher percentages of Al_2O_3 than the round dark gray zones (Point 2 in Fig. 7a). Medium contrast areas have a composition (Point 3 in Fig. 7a) close to the 3:2 mullite that was the initial powders composition. This lack of homogeneity in the local composition of mullite coatings, which has been previously reported by Lee and Miller (Ref 5), is most probably due to the typical rapid cooling rates of the plasma spray process and the incongruent melting of mullite (Ref 3), which obviously precludes recombination of the constituents to crystallize mullite unless subsequent heating of the specimen is carried out. The crystallization of an alumina-rich mullite, typical of mullite grown from melts, has also been suggested as a possible cause of the place to place compositional changes in crystalline mullite coatings (Ref 3-5).

In the ZrO_2-containing coatings, the microstructures become more complex as should be expected. For the M75 layer, zones with small round ZrO_2 grains of about 200 nm are observed (Point 1, Fig. 8a) together with

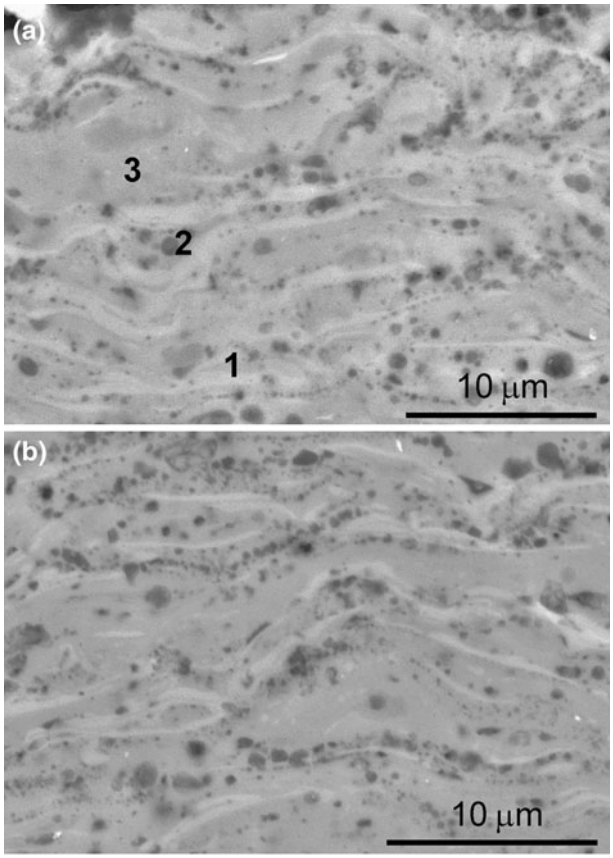

	Al_2O_3 (wt.%)	SiO_2 (wt.%)
Point 1	79	21
Point 2	66	34
Point 3	72	28

Fig. 7 SEM microstructures of M100 coatings: as-sprayed (a) and after 100 h aging (b). Table gives EDS point analysis of representative areas marked in (a) (see text)

Al_2O_3-enriched dark gray pockets (Point 2, Fig. 8a). The matrix (Point 3, Fig. 8a) show a composition close to that originally formulated (Table 2). In the bi-layer coating aged for 100 h (Fig. 8b), the M75 microstructure reflects the widespread nucleation of ZrO_2 grains in the matrix, resembling the typical morphology of solidified eutectic melts. The dark gray features again are Al_2O_3 enriched and ZrO_2 deprived. The M75 microstructure of in the 500 h aged coating is more homogenous (Fig. 8c) with larger ZrO_2 precipitates and fewer Al_2O_3-enriched zones.

In the M50 layer of the as-sprayed three-layer coating (Fig. 9a), similar features to the M75 layer are observed and the same can be said for the corresponding aged specimens. Isolated Al_2O_3-rich areas (Point 1 in Fig. 9a), ZrO_2-rich zones (Point 2 in Fig. 9a) and the continuous phase (Point 3 in Fig. 9a) with composition close to the average (Table 3) are seen. It is noticeable that the microstructure of the 500 h aged M50 layer is similar to the microstructure of a sintered composite of lath-like mullite grains embedded in a ZrO_2 matrix (Fig. 9c).

As happened for the single-layer mullite coatings, neither porosity nor microcraking was observed in the bi- and

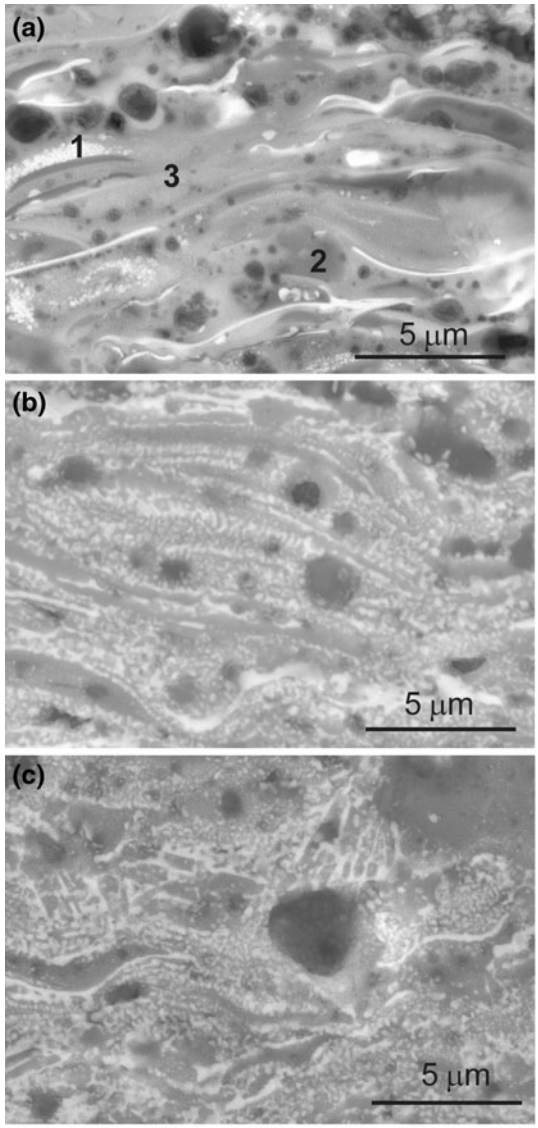

	Al_2O_3 (wt.%)	SiO_2 (wt.%)	Y_2O_3 (wt.%)	ZrO_2 (wt.%)
Point 1	23	11	3	63
Point 2	53	12	3	32
Point 3	43	12	3	41

Fig. 8 SEM microstructures of M75 in the bi-layer coatings: as-sprayed (a), after 100 h aging (b) and after 500 h aging (c). Table gives EDS point analysis of representative areas marked in (a) (see text)

three-layer coatings. Besides, no porous scale formation is perceived as a suggestion of massive volatilization.

For the present exposure conditions, the silica reacting according to reaction (1) to form the zircon phase probably evolves from Al_2O_3/SiO_2 regions where the mullite composition is unbalanced, as these would be amorphous and relatively less stable than stoichiometric mullite. The formation of zircon in the aged specimens somehow avoids the expected silica volatilization from the residual amorphous areas remaining in the coatings.

Another microstructural change is observed in the aged specimens when the substrate/M100 layer interface is

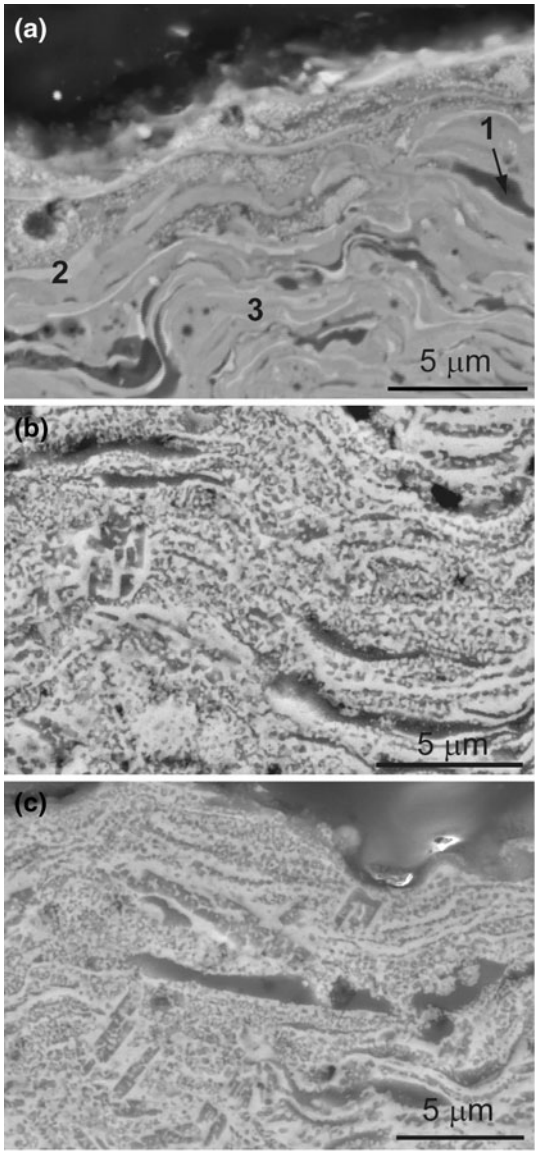

	Al_2O_3 (wt.%)	SiO_2 (wt.%)	Y_2O_3 (wt.%)	ZrO_2 (wt.%)
Point 1	43	6	4	47
Point 2	19	6	5	70
Point 3	25	6	5	64

Fig. 9 SEM microstructures of M50 in the three-layer coatings: as-sprayed (a), after 100 h aging (b) and after 500 h aging (c). Table gives EDS point analysis of representative areas marked in (a) (see text)

analyzed. At this interface, a thin interlayer attached to both the SiC and the mullite layer is observed (Fig. 10). The thickness of this interlayer is given in Table 4, for the different EBC architectures after aging. To get a more clear perspective of affecting factors, data for a single M100-type FG layer and a bi-layer coating (M100 FG/M75) are also specified in the table. It can be seen that the thickness of this layer directly depends on the coating thickness, its porosity, and specific architecture.

EDS point analysis at different locations in the scale give compositions between 70-90 wt.% of SiO_2 depending

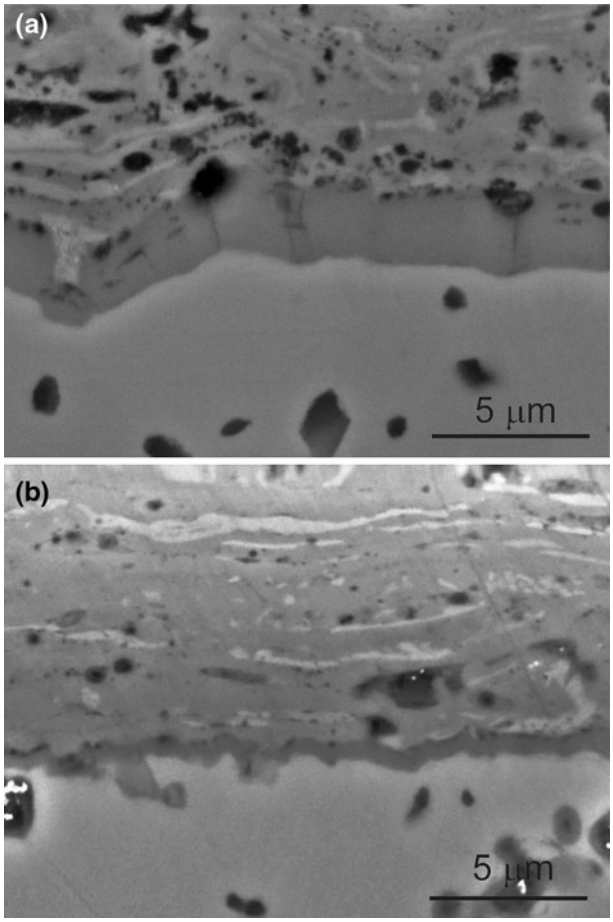

Fig. 10 SEM details of the interface with the SiC substrate in M100 single layer (a) and bi-layer (b) coatings after 100 h aging showing the silica oxidation scale

on the proximity to the adjoined layers, which interfere in the microanalyses. Therefore, this scale is pure silica and is a result of the high temperature oxidation of the SiC substrate by the oxidant atmosphere. Oxygen can reach the substrate through the cracks or by diffusion. In order to verify the crystallinity of the interlayer, a polished cross section of the M100 single-layer coating aged during 100 h was etched with HF acid. In Fig. 11, the comparison of the microstructures for the same region shows that the SiO_2 interface is completely leached out. It can then be concluded that the interlayer is vitreous. Conversely, the adjoining mullite layer does not show noticeable changes apart from some etching at some residual zones (like those pointed in Fig. 11), which are not indicative of the presence of massive amorphous phase in the coatings. Vertical cracks are detected in the silica scale (Fig. 10) specially for the thickest (~6 μm) interlayer, which probably develop to release stresses produced by the lower thermal expansion coefficient of silica compared to the adjacent layers. Nevertheless, massive porosity formation is not observed in the silica scale for the graded coatings. The same occurs for the single-layer mullite coating, but in this case aging extended for only 100 h. For the graded coatings aged

Table 4 Thickness of the silica scale the SiC/mullite interface for different EBC architectures after indicated aging times

	Coating thickness, μm	100 h/1300 °C 90% H_2O	Coating thickness, μm	500 h/1300 °C 90% H_2O
M100	138 ± 12	2 ± 0.8		
M100FG	66 ± 14	3 ± 1.2		
M100/M75	166 ± 5	1.5 ± 1	166 ± 16	5 ± 2
M100FG/M75	146 ± 8	2.5 ± 0.4	167 ± 14	6.5 ± 1.1
M100FG/M75/M50	220 ± 17	1.3 ± 0.3	222 ± 8	6 ± 1.2

Coating thickness of each specimen is given. FG indicates mullite coatings sprayed from FG batch (see text)

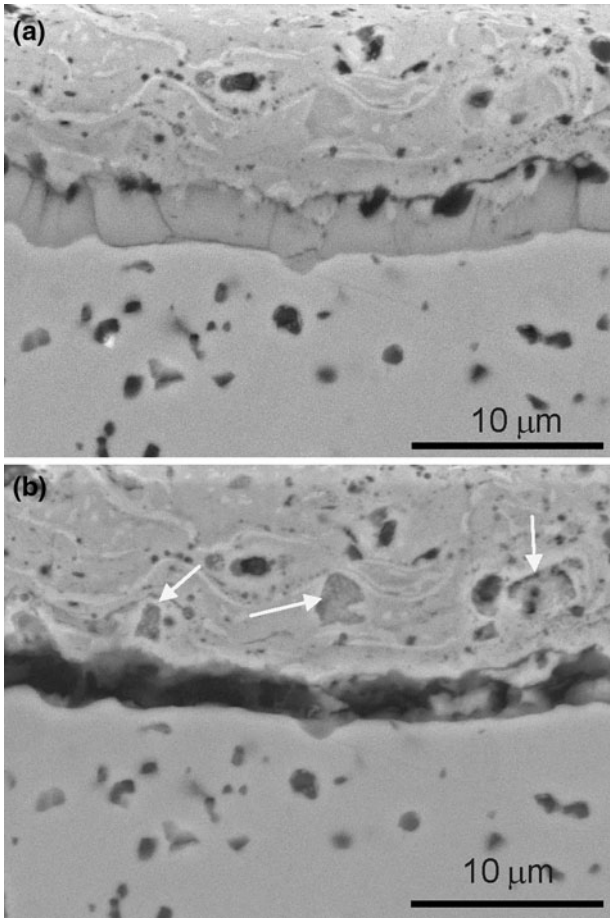

Fig. 11 SEM views of the silica scale in the M100 single coating (aged for 100 h) before (a) and after (b) etching in HF acid. Arrows show the minor etching effect in the mullite coating

during 500 h, some cracks were occasionally seen along the interface with either SiC or mullite, which seems a limiting factor that would need to be tackled in following designs.

4. Conclusions

Mullite-ZrO_2 composite coatings plasma sprayed over SiC substrates showed a relatively good adherence between layers and with the substrate, although evenly spaced vertical cracks were detected. A consistent silica deficit was measured for the mullite-ZrO_2 composite coatings in the as-sprayed conditions, which is linked to the lower refractoriness of these composite coatings, as compared to the pure mullite coatings. Aging at high temperatures and under steam conditions produced a continuous dense vitreous silica oxidation scale between the SiC and the mullite layer. The formation of some zircon observed after 100 h of aging in the composite coatings seems to avoid the silica volatilization.

Acknowledgments

This study has been supported by NRC-CSIC program (project 2007CA003) and MICINN (Ministry of Science and Innovation, Spain) under projects MAT2006-07118 and MAT2009-09600. One of the authors (Eugenio Garcia) acknowledges the Ramón y Cajal Program (MICINN) for the financial support.

References

1. J. Kimmel, N. Miriyala, J. Price, K. More, P. Tortorelli, H. Eaton, G. Linsey, and E. Sun, The Evaluation of CFCC Liners with EBC after Field Testing in a Gas Turbine, *J. Eur. Ceram. Soc.*, 2002, **22**, p 2769-2775
2. I. Spitsberg and J. Steibel, Thermal and Environmental Barrier Coatings for SiC/SiC CMCs in Aircraft Engine Applications, *Int. J. Appl. Ceram. Technol.*, 2004, **1**, p 291-301
3. K.N. Lee, R.A. Miller, and N.S. Jacobson, New Generation of Plasma-Sprayed Mullite Coatings on Silicon Carbide, *J. Am. Ceram. Soc.*, 1995, **78**, p 705-710
4. K.N. Lee and R.A. Miller, Oxidation Behavior of Mullite-Coated SiC and SiC/SiC Composites under Thermal Cycling Between Room Temperature and 1200°-1400°C, *J. Am. Ceram. Soc.*, 1996, **79**, p 620-626
5. K.N. Lee, Key Durability Issues With Mullite-Based Environmental Barrier Coatings for Si-Based Ceramics, *J. Eng. Gas Turbine Power*, 2000, **122**, p 632-636
6. K.N. Lee, D.S. Fox, and N.P. Bansal, Rare earth silicate environmental barrier coatings for SiC/SiC composites and Si_3N_4 ceramics, *J. Am. Ceram. Soc.*, 2005, **25**, p 1705-1715
7. S. Ueno, D.D. Jayaseelan, and T. Ohji, Development of Oxide-Based EBC for Silicon Nitride, *Int. J. Appl. Ceram. Technol.*, 2004, **1**, p 362-373
8. K.N. Lee, D.S. Fox, J.I. Eldrige, D. Zhu, R.C. Robinson, N.P. Bansal, and R.A. Miller, Upper Temperature Limit of Environmental Barrier Coatings Based on Mullite and BSAS, *J. Am. Ceram. Soc.*, 2003, **86**, p 1299-1306

9. S. Ueno, T. Ohji, and H.-T. Lin, Recession behavior of a silicon nitride with multi-layered environmental barrier coating system, *Ceram. Int*, 2007, **33**, p 859-862
10. E. Withey, C. Petorak, R. Trice, G. Dickinson, and T. Taylor, Design of 7 wt.% Y_2O_3-ZrO_2/ mullite plasma-sprayed composite coatings for increased creep resistance, *J. Eur. Ceram. Soc.*, 2007, **27**, p 4675-4683
11. E. Garcia, J. Mesquita-Guimarães, P. Miranzo, M.I. Osendi, Y. Wang, R.S. Lima, and C. Moreau, Mullite and Mullite/ ZrO2-7wt.%Y2O3 Powders for Thermal Spraying of Environmental Barrier Coatings, *J. Therm. Spray Tech.*, 2010, **19**, p 286-293
12. A.D. Jadhav and N.P. Padture, Mechanical Properties of Solution-precursor Plasma-Sprayed Thermal Barrier Coatings, *Surf. Coat. Technol.*, 2008, **202**, p 4976-4979
13. E. Garcia, J. Mesquita-Guimarães, P. Miranzo, and M.I. Osendi, Crystallization Studies In Mullite and Mullite-YSZ Beads, *J. Eur. Ceram. Soc.*, 2010, **30**, p 2003-2008
14. C. Cano, E. Garcia, A.L. Fernandes, M.I. Osendi, and P. Miranzo, Mullite/ZrO_2 Coatings Produced by Flame Spraying, *J. Eur. Ceram. Soc.*, 2008, **28**, p 2191-2197
15. P. Pena and S. De Aza, The Zircon Thermal Behaviour: Effect of Impurities, *J. Mater. Sci.*, 1984, **19**, p 135-142
16. D.R. Spearing and J.Y. Huang, Zircon Synthesis Via Sintering of Milled SiO_2 and ZrO_2, *J. Am. Ceram. Soc.*, 1998, **81**, p 1964-1966
17. K.M. Trappen and R.A. Epplen, Reaction of Zirconia With Silica at the Stoichiometry of Zircon, *J. Am. Ceram. Soc.*, 1889, **72**, p 882-885
18. K.A. Khor and Y. Li, Crystallization Behaviors in the Plasma-Spheroidized Alumina/Zircon Mixtures, *Mater. Lett.*, 2001, **48**, p 57-63